Computers and Structures 320 (2026) 108039

Contents lists available at ScienceDirect

Computers and Structures

journal homepage: www.elsevier.com/locate/cas

On the direct numerical computation of Hopf bifurcations to assess the dynamic stability of fluid-conveying cantilevered pipes

Hauke Gravenkamp [a,*], Bor Plestenjak [b]

[a] Institute of Materials, Technologies and Mechanics, Otto von Guericke University Magdeburg, 39106 Magdeburg, Germany
[b] IMFM and Faculty of Mathematics and Physics, University of Ljubljana, Jadranska 19, SI-1000 Ljubljana, Slovenia

ARTICLE INFO

Keywords:
Pipe
Euler-Bernoulli beam
Stability
Hopf bifurcation
Multiparameter eigenvalue problem
Spectral element method

ABSTRACT

In the structural analysis of fluid-conveying pipes, dynamic instabilities can occur at specific values of the flow velocity, depending on the geometry as well as the material parameters of the pipe and the interior fluid. These critical points fall into the broader category of Hopf bifurcations. Typical numerical models of this problem employ a one-dimensional weighted residual method, leading to a velocity-dependent eigenvalue problem. The solutions form eigencurves, and the critical points are characterized by eigenvalues with vanishing real parts. In this paper, we show that critical points can be computed directly as solutions to a single three-parameter eigenvalue problem. In addition, we employ a recently developed method for computing individual eigencurves, based on the concept of exponential residual relaxation. For the discretization of the weak form, we use a finite element method with a particular version of C^1-continuous high-order spectral elements, suited for fourth-order differential equations, and we discuss the differences compared to the more commonly used weighted residual method based on the basis functions of a linear Euler-Bernoulli beam. Four numerical examples demonstrate the effectiveness of the implemented algorithms. For verification, we provide a detailed derivation of analytical solutions for special cases.

1. Introduction

We address the numerical solution of a classical problem in mechanics, namely, the emergence of instabilities in fluid-conveying pipes. This phenomenon has been known for decades and has been the subject of theoretical [1–3] and experimental studies [4,5]. Such instabilities arise from the interaction between the structural dynamics of the pipe and the momentum of the internal fluid. As the fluid flows through the deformable structure, any lateral deflection of the pipe leads to a change in the fluid's direction of motion. Due to the conservation of momentum, this change generates additional forces that act back on the structure. At low velocities, these forces are relatively small and merely shift the natural frequencies of the system. However, above a certain flow velocity, the feedback between the fluid-induced forces and the structural motion can become destabilizing. The critical velocity above which an instability occurs is related to the existence of a Hopf bifurcation, where a pair of complex-conjugate eigenvalues cross the imaginary axis as a parameter is varied, leading to a qualitative change in the system's behavior.[1] Bifurcations of this kind play a crucial role in various engineering systems beyond the one already described and can lead to flow-induced instabilities such as aeroelastic flutter. Similar dynamical phenomena also occur, e.g., in gyroscopic systems [6]. The general theoretical framework for analyzing flow-induced instabilities and bifurcations has been laid out in foundational works such as [2]. A more specific treatment of Hopf bifurcations in fluid-conveying pipes can be found in [7], which presents a fundamental description of the dynamics. This has since been extended to more general nonlinear models and linear stability analyses of particular cases [8], including related configurations such as spring-supported pipes [9] and cantilevered pipes with time delay [10].

These models typically rely on a one-dimensional representation of the pipe, with the effects of the fluid motion incorporated as internal

* Corresponding author.
Email addresses: hauke.gravenkamp@ovgu.de (H. Gravenkamp), bor.plestenjak@fmf.uni-lj.si (B. Plestenjak).

[1] While Hopf bifurcations are typically defined at points where the eigenvalues cross the real axis, we will state the problem in such a way that the eigenvalues cross the imaginary axis. The difference is just a convention, but it leads, in our case, to the eigenvalue problem being real-valued, hence improving the efficiency of its numerical solution.

https://doi.org/10.1016/j.compstruc.2025.108039
Received 4 September 2025; Accepted 8 November 2025
Available online 19 November 2025

forces. A weighted residual method is commonly employed to derive a parameter-dependent eigenvalue problem of the form $\mathbf{L}(\nu,u)\boldsymbol{\eta}=\mathbf{0}$, where ν is the eigenvalue, $\boldsymbol{\eta}$ the corresponding eigenvector, and u the (dimensionless) flow velocity. Here, $\mathbf{L}(\nu,u)$ is introduced as a generic matrix function to be specified later. Computing the eigenvalues for a range of flow velocities yields *eigencurves*. Instabilities are, in this setting, associated with the occurrence of eigenvalues with vanishing real parts. The flow velocity at which this condition is met is referred to as the critical velocity u_c, and the associated pair (u_c,ν_c) defines a critical point, where ν_c is the critical eigenvalue. Traditionally, such critical points are determined by evaluating the eigencurves over a range of velocities and identifying the locations where the real part of an eigenvalue crosses zero. Rather than computing all eigenvalues at a set of predefined discrete velocities, it is possible to follow individual eigencurves continuously by updating the eigenvalue as a function of velocity. This approach has been suggested for this application by Wagner [11], who proposed a continuation method to compute selected eigencurves.

In this work, we discuss how to directly compute these critical points by solving only one (albeit larger) eigenvalue problem without tracking any of the eigencurves. Such strategies have been known to work for specific problems; see, e.g., [12], where the larger eigenvalue problem was constructed directly as a Kronecker product of the involved matrices. Similar solution procedures have been presented in the context of aeroelastic flutter analysis [13–16]. In our case, the key observation is that, at Hopf bifurcation points, both ν_c and $-\nu_c$ are eigenvalues corresponding to the same velocity u_c. Consequently, critical points satisfy both equations $\mathbf{L}(\nu_c,u_c)\,\boldsymbol{\eta}_1=\mathbf{0}$ and $\mathbf{L}(-\nu_c,u_c)\,\boldsymbol{\eta}_2=\mathbf{0}$ simultaneously. This statement can be written in the form of a *multiparameter eigenvalue problem* in the unknowns ν and u, additionally taking into account the quadratic terms in both parameters. In fact, the eigenvalue problem in this application exhibits a particularly interesting structure, allowing us to recast it in terms of the three parameters ν^2, u^2, and $u\nu$. Efficient algorithms for solving such multiparameter eigenvalue problems are available [17,18], and implementations can be found in the open-source Matlab toolbox *MultiParEig* [19]. Utilizing this approach enables the simultaneous computation of all critical points by solving a single, larger eigenvalue problem involving the so-called operator determinants. We have previously employed related techniques for locating zero group velocity points in elastic waveguides, which are again points on eigencurves that satisfy specific constraints [20,21]. In [22], we demonstrated how certain nonlinear, parameter-dependent eigenvalue problems can be efficiently reformulated and solved via a multiparameter framework.

While critical points often represent the most significant features of such potentially unstable systems, in some cases, it remains desirable to compute eigencurves across a range of flow velocities. Usually, only a few modes—particularly those that exhibit critical behavior—are of interest. In this context, we present a recently developed technique that serves as an alternative to continuation-based approaches like that of Wagner [6,11]. It transforms the eigenvalue problem into a system of ordinary differential equations by assuming an exponentially decaying residual. This approach will hence be referred to as *exponential residual relaxation* throughout this work. Given a known solution at some reference velocity u_0 (for instance, a critical point), the evolution of the eigenpair with changing velocity can be treated as an initial value problem, which can be efficiently solved using standard Runge-Kutta-type integrators. This concept was, in this form, introduced by Zhang et al. [23–25] and has since been adapted to broader classes of matrix equations by Uhlig and co-workers [26–28]. In [29,30], we demonstrated its effectiveness for tracing eigencurves in the context of elastic guided wave modeling, employing semi-analytical models as described, e.g., in [22,31,32].

In addition to the numerical strategies for solving the eigenvalue problems, we provide a detailed discussion of the finite element discretization used for the pipe system. Classical formulations typically rely on a weighted residual approach using the eigenfunctions of a vibrating Euler-Bernoulli beam as basis functions. In contrast, we propose a more general finite element scheme based on polynomial shape functions of arbitrary degree. Due to the fourth-order nature of the governing equations, C^1-continuous elements are required; specifically, we employ a class of high-order spectral elements recently discussed in [33,34].

In summary, this paper entails the following novel contributions:

- A method for the direct computation of critical points in fluid-conveying pipes.
- The application of exponential residual relaxation for computing individual modes in the current application.
- The application of recently developed high-order beam elements to this problem class.

The remainder of this paper is structured as follows: In Section 2, we describe the physical system and state the boundary value problem. Section 3 covers the derivation of the weak form and its discretization using the finite element method. The direct computation of critical points via the multiparameter eigenvalue formulation is presented in Section 4. Section 5 introduces the exponential residual relaxation method for tracing eigencurves. Numerical examples are given in Section 6, and concluding remarks are provided in Section 7. Analytical solutions for special cases used for verification are included in the appendix.

2. Problem statement

We address a cantilevered pipe, conveying a fluid with flow velocity v as shown in Fig. 1. The notation is adopted from [11]; details on the derivation of the partial differential equation (PDE) describing this problem can be found there and, in more detail, in [7]. As our contributions concern solely the *solution* of this PDE, we will refrain from repeating details of the derivation and directly pose the final boundary value problem: For given u,β,γ, find $\hat{\eta}=\hat{\eta}(\xi,t)$ such that

$$\hat{\eta}''''+u^2\hat{\eta}''+\gamma(\xi-1)\hat{\eta}''+2\sqrt{\beta}u\dot{\hat{\eta}}'+\gamma\hat{\eta}'+\ddot{\hat{\eta}}=0,\qquad \xi\in(0,1) \tag{1}$$

subject to the boundary conditions

$$\hat{\eta}(0)=0,\quad \hat{\eta}'(0)=0\qquad \text{(Dirichlet)}, \tag{2a}$$

$$\hat{\eta}''(1)=0,\quad \hat{\eta}'''(1)=0\qquad \text{(von Neumann)}. \tag{2b}$$

Eq. (1) is presented in a non-dimensional form, using the following quantities

$$\xi=\frac{x}{L},\qquad \hat{\eta}=\frac{w}{L},\qquad \tau=\sqrt{\frac{EI}{m_f+m_p}}\,\frac{t}{L^2},\qquad u=\sqrt{\frac{m_f}{EI}}\,vL,$$

$$\gamma=\frac{m_p+m_f}{EI}L^3\,g,\qquad \beta=\frac{m_f}{m_p+m_f}>0$$

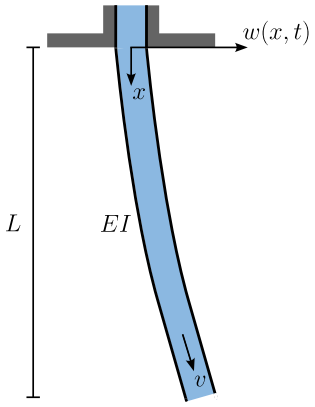

Fig. 1. Sketch of a cantilevered fluid-conveying pipe.

with the symbols defined as follows

x:	spatial coordinate in axial direction,
ξ:	dimensionless coordinate,
t:	time,
τ:	dimensionless time,
L:	pipe length,
E:	Young's modulus,
I:	area moment of inertia,
m_f:	fluid mass per unit length,
m_p:	pipe mass per unit length,
v:	flow velocity,
u:	dimensionless flow velocity,
w:	deflection,
$\hat{\eta}$:	dimensionless deflection,
g:	gravitational acceleration in x-direction.

Correspondingly, the prime and dot symbols denote derivatives with respect to the dimensionless variables ξ and τ. Note that the behavior of the fluid-conveying pipe is characterized by the two problem-dependent parameters β and γ, which are associated with the mass ratio of fluid and pipe and the force ratio of tension and flexural restoring force, respectively.[2] Substituting a time dependency

$$\hat{\eta}(\xi,\tau) = \eta(\xi)\exp(\nu\tau) \tag{3}$$

yields the corresponding ordinary differential equation for the dimensionless deflection amplitudes η:

$$\eta'''' + u^2\eta'' + \gamma(\xi-1)\eta'' + 2\sqrt{\beta}u\nu\eta' + \gamma\eta' + \nu^2\eta = 0. \tag{4}$$

Assume γ, β are fixed for a given physical setup. We are interested in the set of eigenvalues ν_i and corresponding eigenfunctions $\eta_i(\xi)$ ($i \in \mathbb{N}$) and their behavior when varying the flow velocity u. In particular, the system is unstable at a given u if $\Re(\nu_i) > 0$ for any of the eigenvalues. Hence, values of u where the real part of any of the eigenvalues vanishes are referred to as the critical velocity u_c.

3. Finite-element formulation

3.1. Weak form and discretization

In order to obtain a spatial discretization of Eq. (4) by means of the finite element method, we multiply by test functions ζ and integrate over the computational domain

$$(\zeta,\eta'''') + (u^2-\gamma)(\zeta,\eta'') + \gamma(\zeta,\xi\eta'') + \gamma(\zeta,\eta') + 2\sqrt{\beta}u\nu(\zeta,\eta') + \nu^2(\zeta,\eta) = 0, \tag{5}$$

where we use $(a,b) = \int_0^1 ab\,\mathrm{d}\xi$ to denote integration over the computational domain, irrespective of whether this operation corresponds to an L_2 inner product. We integrate by parts the first term twice and drop the resulting boundary terms for conciseness, as they vanish in the case of the boundary conditions stated above. Hence, the weak form reads

$$(\zeta'',\eta'') + (u^2-\gamma)(\zeta,\eta'') + \gamma(\zeta,\xi\eta'') + \gamma(\zeta,\eta') + 2\sqrt{\beta}u\nu(\zeta,\eta') + \nu^2(\zeta,\eta) = 0. \tag{6}$$

We may note that we could also integrate by parts one of the terms that involves η'' and one of the terms that involves η' to obtain a more symmetric structure of the final equations. While this may be advantageous for large problems, we refrain from doing so here for simplicity and to avoid additional boundary contributions. To arrive at a finite element approximation of the weak form, we choose adequate finite element spaces and replace the trial and test functions with their discrete counterparts

$$\eta_h = \sum_{i=1}^{N}\psi_i(\xi)\,\eta_i, \qquad \zeta_h = \sum_{i=1}^{N}\psi_i(\xi)\,\zeta_i, \tag{7}$$

where $\psi_i(\xi)$ are the basis functions ('shape functions'), and η_i, ζ_i denote the corresponding coefficients (unknowns). Hence, the finite element formulation becomes

$$\begin{aligned}&(\zeta_h'',\eta_h'') + (u^2-\gamma)(\zeta_h,\eta_h'') + \gamma(\zeta_h,\xi\eta_h'') + \gamma(\zeta_h,\eta_h')\\ &\quad + 2\sqrt{\beta}u\nu(\zeta_h,\eta_h') + \nu^2(\zeta_h,\eta_h) = 0.\end{aligned} \tag{8}$$

Here, we assume the use of the same basis functions ψ_i for approximating the trial and test functions (Bubnov-Galerkin approach). The solution vector containing all coefficients η_i will be denoted as $\boldsymbol{\eta}$. Performing the integrations in Eq. (8) finally yields the matrix equation

$$\mathbf{L}(\nu,u)\boldsymbol{\eta} := \nu^2\mathbf{M}\boldsymbol{\eta} + \nu\mathbf{C}(u)\boldsymbol{\eta} + \mathbf{K}(u)\boldsymbol{\eta} = \mathbf{0} \tag{9}$$

with

$$\mathbf{C}(u) = 2\sqrt{\beta}u\mathbf{B}, \tag{10}$$

$$\mathbf{K}(u) = \mathbf{A} + (u^2-\gamma)\mathbf{G} + \gamma(\mathbf{D}+\mathbf{B}) \tag{11}$$

and the matrix function $\mathbf{L}(\nu,u)$ defined for later use. The entries of the matrices $\mathbf{A}$, $\mathbf{B}$, $\mathbf{D}$, $\mathbf{G}$, and $\mathbf{M}$ are given as:

$$\begin{aligned}A_{ij} &= \int_0^1 \psi_i''\psi_j''\,d\xi, \qquad B_{ij} = \int_0^1 \psi_i\psi_j'\,d\xi,\\ D_{ij} &= \int_0^1 \xi\psi_i\psi_j''\,d\xi, \qquad G_{ij} = \int_0^1 \psi_i\psi_j''\,d\xi, \qquad M_{ij} = \int_0^1 \psi_i\psi_j\,d\xi.\end{aligned} \tag{12}$$

Note that we have assumed, for simplicity, that the properties of the pipe, β, γ, are independent of the spatial coordinate ξ, allowing us to perform the integrations independently of the problem data. The same assumption has been made in [7,11]. For a given u, Eq. (9) poses a quadratic eigenvalue problem (QEP), whose solutions are eigenvalues ν and discretized mode shapes $\boldsymbol{\eta}$. The solutions can be obtained using standard algorithms, often after first transforming the quadratic eigenvalue problem into a standard generalized eigenvalue problem by means of a companion linearization. Computing the eigenvalues $\nu_i(u)$ for a set of discrete values of u leads to the *eigencurves*, i.e., they provide information on how each eigenfrequency varies under the influence of the flow velocity u. As mentioned before, there are alternatives to directly computing all eigenvalues for each of the a priori defined u-values, i.e., methods to follow individual eigencurves by a continuation approach [11,35] or by solving a differential equation describing the residual of the eigenvalue problem [29,30], as we will discuss in Section 5.

3.2. Choice of shape functions

To solve this particular boundary value problem, it seems common to use the modes of vibration of the homogeneous Euler-Bernoulli cantilever beam as basis functions [1,8,11]. These are given by

$$\psi_i^{\mathrm{EB}}(\xi) = \cosh\lambda_i\xi - \cos\lambda_i\xi - \frac{\sinh\lambda_i - \sin\lambda_i}{\cosh\lambda_i + \cos\lambda_i}\left(\sinh\lambda_i\xi - \sin\lambda_i\xi\right), \tag{13}$$

where each λ_i solves the transcendental equation

$$1 + \cos\lambda_i\cosh\lambda_i = 0. \tag{14}$$

The use of this basis is motivated by the fact that the differential equation still shows resemblance to that describing the Euler-Bernoulli beam – even though it involves additional terms, making the problem significantly more complex. From the standpoint of more general

[2] The dimensionless parameter γ involves the gravitational acceleration in axial direction and, hence, depends on the pipe's orientation. According to the convention employed here, $\gamma > 0$ implies that (a component of) the gravitational acceleration acts in the direction of the fluid flow velocity, whereas $\gamma = 0$ represents a horizontal pipe. We also assume $\beta > 0$, i.e., the fluid's density cannot be neglected.

weighted residuals or finite element methods, employing these basis functions is a rather unconventional choice, and many readers may wonder about the effectiveness of this approach. In fact, while the resulting finite-element formulation does give surprisingly accurate results, these basis functions come with several disadvantages. First of all, as they are eigenfunctions of the much simpler equation $\eta'''' + \eta = 0$, it is not immediately obvious how well they will approximate solutions of Eq. (4), especially in view of the additional term in $\xi\eta''$. In other words, the typical a priori error estimators well established in standard finite element theory do not directly apply, and the asymptotic convergence rate is lower compared to polynomial interpolants. In addition, it is essential to note that the transcendental Eq. (14) needs to be solved numerically and with high accuracy for each value of λ_i to obtain this basis. Finding all solutions up to a given number of desired basis functions can in itself be a rather challenging task. We may also point out that this basis holds for exactly the boundary conditions of a cantilevered beam (as given in Eqs. (2)); i.e., they have to be adapted for different boundary data. This restriction also implies that we cannot subdivide the geometry into several elements in this manner, as these basis functions would not satisfy continuity of the deflection at element interfaces. If we perform the integrations in Eqs. (12) numerically, care must be taken when evaluating the potentially huge terms in cosh and sinh. However, if all properties of the pipe and the fluid are constant along ξ (as has been assumed before), simple analytical expressions can be derived for the entries of the finite element matrices, owing to the orthonormality of this basis. These expressions are listed in [11]. Still, the resulting matrices are prone to ill-conditioning, as their entries can span many orders of magnitude, depending on the number of modes included in the computation.

Because of the difficulties mentioned above, we prefer to use a more conventional polynomial basis, as is common in most applications of the finite element method. As the differential equation is of fourth order, we require basis functions with continuous derivatives (C^1 continuity), such that the finite element functions belong to the Sobolev space H^2. The typical choice (well-known from standard beam elements) is Hermite polynomials of order three, which are constructed by enforcing

$$\begin{aligned}
&\psi_1(0) = 1, \quad \psi_1(1) = \psi_1'(0) = \psi_1'(1) = 0,\\
&\psi_2(1) = 1, \quad \psi_2(0) = \psi_2'(0) = \psi_2'(1) = 0,\\
&\psi_3'(0) = 1, \quad \psi_3(0) = \psi_3(1) = \psi_3'(1) = 0,\\
&\psi_4'(1) = 1, \quad \psi_4(0) = \psi_4(1) = \psi_4'(0) = 0.
\end{aligned} \tag{15}$$

The four degrees of freedom of the resulting element are the values of the solution and its slope at the element endpoints. The same concept can be extended straightforwardly to polynomials of higher order, as has been discussed in the literature rather recently [33,34]. To this end, we include additional nodes inside the element, e.g., at the Gauss-Lobatto points for improved robustness. Each node increases the number of degrees of freedom by two and requires two additional shape functions whose value and slope, respectively, equal one at the node. These basis functions define a natural extension of the well-known *spectral element* – the C^0-continuous counterpart often used to solve variants of the wave equation in acoustics, elasticity, or electromagnetism, see, e.g., [36–38]. In our numerical examples in Section 6, we compare both approaches and observe that the 'beam modes' perform better than one may expect for the problem at hand; however, the polynomial basis functions lead to significantly faster error convergence.

4. Direct computation of critical points

We now shift our attention to the solution of Eq. (9), in particular, the computation of critical points. In our setup, critical points (u_c, v_c) are points on an eigencurve where the real part of the eigenvalue vanishes.[3]

We will see that these critical points are solutions to a multiparameter eigenvalue problem that can be solved using available algorithms. The key is to notice that, since the matrices $\mathbf{M}, \mathbf{C}(u), \mathbf{K}(u)$ are real-valued, any complex (including purely imaginary) eigenvalues occur in conjugate pairs, i.e., if $\mathbf{L}(v,u)\boldsymbol{\eta} = \mathbf{0}$ then also $\mathbf{L}(\overline{v},u)\overline{\boldsymbol{\eta}} = \mathbf{0}$. Hence, in the case of purely imaginary eigenvalues (such as the critical points), v and $-v$ are both solutions. Thus, critical points must simultaneously solve both equations

$$\mathbf{L}(+v,u)\boldsymbol{\eta}_1 = \mathbf{0}, \tag{16a}$$

$$\mathbf{L}(-v,u)\boldsymbol{\eta}_2 = \mathbf{0}. \tag{16b}$$

Eqs. (16) define a two-parameter eigenvalue problem, i.e., a set of two eigenvalue problems for two unknowns. If v, u and nonzero $\boldsymbol{\eta}_1$, $\boldsymbol{\eta}_2$ satisfy (16), then (v,u) is an eigenvalue, and $\boldsymbol{\eta}_1 \otimes \boldsymbol{\eta}_2$ is the corresponding eigenvector. Hence, if (u_c, v_c) is a critical point of (9), and $\boldsymbol{\eta}_c$ is the corresponding eigenvector such that $\mathbf{L}(v_c,u_c)\boldsymbol{\eta}_c = \mathbf{0}$, then (v_c,u_c) is an eigenvalue of (16), and $\boldsymbol{\eta}_c \otimes \overline{\boldsymbol{\eta}_c}$ is the eigenvector. In addition to the critical points, there can be other eigenvalues of the two-parameter eigenvalue problem (16); hence, the critical points will be selected in a postprocessing step. We assume that the problem is such that all critical points are isolated. Notably, if we allow $\beta = 0$ (corresponding to a massless fluid), the linear term in Eq. (9) vanishes; hence, in this unphysical case, *all* eigenvalues satisfy both Eq. (16). However, this case exhibits modes that are purely imaginary for any u but no critical points in the sense discussed here.

The Eqs. (16) are quadratic in both u and v and should be linearized for an efficient solution. In general, one can employ a companion linearization for this purpose, as shown in [18], which would lead to a linear two-parameter eigenvalue problem with matrices of size $3N \times 3N$. It should be noted that, in addition to returning very large matrices, this approach also results in a singular problem, which is significantly more challenging to solve numerically than a regular one.

On the contrary, our finite-element model leads to a regular problem for the critical points. We can exploit the fact that the problem at hand exhibits a specific structure, allowing a particularly efficient reformulation, where, in the same way as in [15] for a similar problem, we employ a strategy referred to as *quasi-linearization* (based on the terminology introduced in [39]) by introducing additional parameters representing higher monomial orders of v and u. As the eigenvalue problem only involves terms in v^2, vu, and u^2 (that is to say, no terms in u or v individually), we can rewrite (16) as a three-parameter eigenvalue problem, denoting the parameters as

$$\alpha_1 = v^2, \quad \alpha_2 = uv, \quad \alpha_3 = u^2. \tag{17}$$

Consequently, in addition to Eqs. (16), we introduce one equation that defines the relationship between α_1, α_2, and α_3, leading to the three-parameter eigenvalue problem:

$$\left(\alpha_1 \begin{bmatrix} 1 & 0 \\ 0 & 0 \end{bmatrix} + \alpha_2 \begin{bmatrix} 0 & 1 \\ 1 & 0 \end{bmatrix} + \alpha_3 \begin{bmatrix} 0 & 0 \\ 0 & 1 \end{bmatrix}\right) \mathbf{x} = \mathbf{0}, \tag{18a}$$

$$\left(\alpha_1\mathbf{M} + 2\alpha_2\sqrt{\beta}\mathbf{B} + \alpha_3\mathbf{G} + \mathbf{A} + \gamma(\mathbf{D} + \mathbf{B} - \mathbf{G})\right)\boldsymbol{\eta}_1 = \mathbf{0}, \tag{18b}$$

$$\left(\alpha_1\mathbf{M} - 2\alpha_2\sqrt{\beta}\mathbf{B} + \alpha_3\mathbf{G} + \mathbf{A} + \gamma(\mathbf{D} + \mathbf{B} - \mathbf{G})\right)\boldsymbol{\eta}_2 = \mathbf{0}. \tag{18c}$$

The first equation defines the relationship $\alpha_1\alpha_3 - \alpha_2^2 = 0$, since

$$\det\left(\alpha_1 \begin{bmatrix} 1 & 0 \\ 0 & 0 \end{bmatrix} + \alpha_2 \begin{bmatrix} 0 & 1 \\ 1 & 0 \end{bmatrix} + \alpha_3 \begin{bmatrix} 0 & 0 \\ 0 & 1 \end{bmatrix}\right) = \det\left(\begin{bmatrix} \alpha_1 & \alpha_2 \\ \alpha_2 & \alpha_3 \end{bmatrix}\right) = \alpha_1\alpha_3 - \alpha_2^2. \tag{19}$$

Details on the solution of such multiparameter eigenvalue problems can be found in [17,18], and applications to other problems of practical relevance are presented in [20–22]. We make use of the open-source Matlab

[3] We deliberately chose $\hat{\eta}(\xi,\tau) = \eta(\xi)\exp(v\tau)$ instead of $\hat{\eta}(\xi,\tau) = \eta(\xi)\exp(\mathrm{i}v\tau)$ in Eq. (3) in order to keep all matrices defining the eigenvalue problem real-valued, thus improving efficiency.

toolbox *MultiParEig* [19] to solve Eq. (18). In a nutshell, the eigenvalues α_i of the three-parameter eigenvalue problem of the form

$$(\mathbf{L}_{10} + \alpha_1\mathbf{L}_{11} + \alpha_2\mathbf{L}_{12} + \alpha_3\mathbf{L}_{13})\,\mathbf{x} = \mathbf{0}, \tag{20a}$$

$$(\mathbf{L}_{20} + \alpha_1\mathbf{L}_{21} + \alpha_2\mathbf{L}_{22} + \alpha_3\mathbf{L}_{23})\boldsymbol{\eta}_1 = \mathbf{0}, \tag{20b}$$

$$(\mathbf{L}_{30} + \alpha_1\mathbf{L}_{31} + \alpha_2\mathbf{L}_{32} + \alpha_3\mathbf{L}_{33})\boldsymbol{\eta}_2 = \mathbf{0} \tag{20c}$$

are solutions of the generalized linear eigenvalue problems

$$\boldsymbol{\Delta}_i\mathbf{z} = \alpha_i\boldsymbol{\Delta}_0\mathbf{z}, \tag{21}$$

where $\mathbf{z} = \mathbf{x} \otimes \boldsymbol{\eta}_1 \otimes \boldsymbol{\eta}_2$ denotes the corresponding eigenvector with the Kronecker product $\otimes$, and the matrices

$$\boldsymbol{\Delta}_0 = \begin{vmatrix} \mathbf{L}_{11} & \mathbf{L}_{12} & \mathbf{L}_{13} \\ \mathbf{L}_{21} & \mathbf{L}_{22} & \mathbf{L}_{23} \\ \mathbf{L}_{31} & \mathbf{L}_{32} & \mathbf{L}_{33} \end{vmatrix}_{\otimes}, \qquad \boldsymbol{\Delta}_1 = -\begin{vmatrix} \mathbf{L}_{10} & \mathbf{L}_{12} & \mathbf{L}_{13} \\ \mathbf{L}_{20} & \mathbf{L}_{22} & \mathbf{L}_{23} \\ \mathbf{L}_{30} & \mathbf{L}_{32} & \mathbf{L}_{33} \end{vmatrix}_{\otimes}, \tag{22a}$$

$$\boldsymbol{\Delta}_2 = -\begin{vmatrix} \mathbf{L}_{11} & \mathbf{L}_{10} & \mathbf{L}_{13} \\ \mathbf{L}_{21} & \mathbf{L}_{20} & \mathbf{L}_{23} \\ \mathbf{L}_{31} & \mathbf{L}_{30} & \mathbf{L}_{33} \end{vmatrix}_{\otimes}, \qquad \boldsymbol{\Delta}_3 = -\begin{vmatrix} \mathbf{L}_{11} & \mathbf{L}_{12} & \mathbf{L}_{10} \\ \mathbf{L}_{21} & \mathbf{L}_{22} & \mathbf{L}_{20} \\ \mathbf{L}_{31} & \mathbf{L}_{32} & \mathbf{L}_{30} \end{vmatrix}_{\otimes}, \tag{22b}$$

are commonly referred to as operator determinants [40]. They are constructed by a generalized Leibniz formula for the determinant, with the Kronecker product instead of the usual product. A multiparameter eigenvalue problem is regular when the operator determinant $\boldsymbol{\Delta}_0$ is nonsingular; otherwise, the problem is singular and much more difficult to solve.

If N is the number of degrees of freedom of our finite element model, the matrices in the original eigenvalue problem are of size $N \times N$, and the operator determinants are of size $2\,N^2 \times 2\,N^2$. The operator determinant $\boldsymbol{\Delta}_0$ corresponding to the problem (18) has block form

$$\boldsymbol{\Delta}_0 = \begin{bmatrix} 2\sqrt{\beta}(\mathbf{B}\otimes\mathbf{G} + \mathbf{G}\otimes\mathbf{B}) & \mathbf{G}\otimes\mathbf{M} - \mathbf{M}\otimes\mathbf{G} \\ \mathbf{G}\otimes\mathbf{M} - \mathbf{M}\otimes\mathbf{G} & -2\sqrt{\beta}(\mathbf{M}\otimes\mathbf{B} + \mathbf{B}\otimes\mathbf{M}) \end{bmatrix},$$

which is clearly nonsingular for the choice $\mathbf{B} = \mathbf{G} = \mathbf{M} = \mathbf{I}_N$, resulting in

$$\boldsymbol{\Delta}_0 = \begin{bmatrix} 4\sqrt{\beta}\,\mathbf{I}_{N^2} & 0 \\ 0 & -4\sqrt{\beta}\,\mathbf{I}_{N^2} \end{bmatrix}.$$

It follows that $\det(\boldsymbol{\Delta}_0)$, which is a polynomial in the entries of matrices $\mathbf{B}, \mathbf{G}$, and $\mathbf{M}$, is not identically zero[4]; thus, (18) is nonsingular for a generic problem (9) and has $2N^2$ solutions $(\alpha_1, \alpha_2, \alpha_3)$. Let us remark that this quasi-linearization can be applied to a generic quadratic two-parameter eigenvalue problem that has no linear monomials v and u, and thus complements the list of quasi-linearizations in [39, Section 5].

Note that the solutions of the initial quadratic eigenvalue problem (16) appear in pairs (v, u) and $(-v, -u)$, because $\mathbf{L}(v, u) = \mathbf{L}(-v, -u)$. As each solution $(\alpha_1, \alpha_2, \alpha_3)$ of (18) corresponds to a pair (v, u) and $(-v, -u)$, we obtain all $4\,N^2$ solutions of (16) from (18).

To compute the critical velocities, it is sufficient to solve one eigenvalue problem $\boldsymbol{\Delta}_3\mathbf{z} = \alpha_3\boldsymbol{\Delta}_0\mathbf{z}$ with $u_c = \sqrt{\alpha_3}$. More precisely, the solutions obtained in this manner are *candidates* for critical velocities, as there may be additional solutions that also satisfy Eq. (21). To ensure the obtained values are meaningful, we simply extract candidate solutions with real-valued, positive velocities.

[4] This follows from a well-known fact in algebraic geometry: The zero set of a polynomial in several variables is either the whole space (if the polynomial is identically zero) or an algebraic set of lower dimension, whose complement is dense and of full measure. To show that the polynomial is not identically zero, it suffices to find a single set of variables for which it evaluates to a nonzero value; in that case, the polynomial vanishes only on an exceptional set, and it takes nonzero values for a generic set of variables. For details, see, e.g., [41].

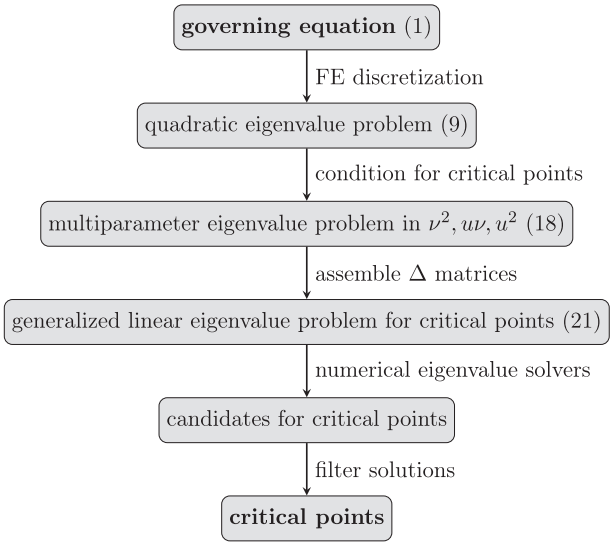

Fig. 2. Flow chart indicating the required steps in obtaining solutions of critical points.

However, it must be acknowledged that the solution to this eigenvalue problem is rather expensive due to the significantly larger matrix size $2N^2 \times 2N^2$ compared to the original $N \times N$ finite element matrices. In our current application, where the geometry is approximated by one-dimensional finite elements, the matrix size is typically small enough so that this method can be applied with ease. For larger matrix sizes, one would have to employ subspace methods; e.g., it may be possible to extend the work presented by Meerbergen and Spence [42]. They showed that a related problem (that is linear in both parameters) can be solved by working only with vectors of order N, i.e., without assembling the operator determinants. Now that we have presented all the ingredients required for the direct computation of critical points, we summarize these steps in Fig. 2 for conciseness.

5. Individual mode computation by exponential residual relaxation

Notwithstanding the fact that we can now directly compute the critical points, it is sometimes desired to obtain the complete eigencurves and study the behavior of individual modes as the flow velocity varies. Finding many discrete solutions can be achieved by solving the quadratic eigenvalue problem (9) successively for a set of pre-defined values of u. This approach leads to a scatter plot of many discrete points in the u-v plane and requires a priori knowledge of an adequate step size in u necessary to resolve all relevant features. Hence, another increasingly popular approach to similar problems is to follow individual eigencurves, computing successive points starting from some initial solution. We present, in the following, one particularly interesting representative of this category of methods that has previously been shown to be very robust for computing eigencurves of general nonlinear eigenvalue problems.

The underlying idea is the following. Given some objective function $f(y(u), u)$ that depends on a parameter u, the goal is to minimize f over a range of values of the parameter, i.e.,

$$f(y(u), u) = 0. \tag{23}$$

We can approximately rewrite the above statement as a simple first-order ordinary differential equation by postulating an exponentially decaying residual:

$$f'(y(u), u) = -\chi f(y(u), u) \tag{24}$$

with a decay parameter χ. Here, the prime symbol denotes a derivative with respect to u. Assuming a solution $y_0(u_0)$ at some value u_0 is known at least approximately, we can solve Eq. (24) numerically using standard algorithms, typically of the Runge-Kutta class. It has previously been observed that this approach performs remarkably well for various problems and a wide range of decay parameters [26–29]. It also tends to converge rapidly to a solution even when the accuracy of the initial guess is extremely low [30]. Further details on this idea can be found in the mentioned references. In particular, the following steps are essentially analogous to the formulation in [30].

Applying this concept to our parameter-dependent eigenvalue problem, we define the objective function

$$\mathbf{f}(\boldsymbol{\eta}(u), \nu(u), u) = \begin{bmatrix} \mathbf{L}(\nu, u)\,\boldsymbol{\eta} \\ \boldsymbol{\eta}^{\mathsf{H}}\boldsymbol{\eta} - 1 \end{bmatrix}, \tag{25}$$

where the second row is a normalization of the eigenvector, necessary to obtain a unique result. To apply Eq. (24), we require the total derivative of the objective function[5] with respect to the parameter u

$$\mathbf{f}'(\boldsymbol{\eta}, \nu, u) = \begin{bmatrix} \mathbf{L}(\nu, u)\boldsymbol{\eta}' + \mathbf{L}'(\nu, u)\boldsymbol{\eta} \\ 2\boldsymbol{\eta}^{\mathsf{H}}\,\boldsymbol{\eta}' \end{bmatrix}. \tag{26}$$

The total derivative of the matrix function $\mathbf{L}(\nu, u)$ is obtained as

$$\mathbf{L}'(\nu, u) = \mathbf{L}_u(\nu, u) + \mathbf{L}_\nu(\nu, u)\,\nu', \tag{27}$$

where $\mathbf{L}_u(\nu, u)$ and $\mathbf{L}_\nu(\nu, u)$ denote the partial derivatives with respect to u and ν. Hence, we obtain

$$\mathbf{f}'(\boldsymbol{\eta}, \nu, u) = \begin{bmatrix} \mathbf{L}(\nu, u)\,\boldsymbol{\eta}' + \mathbf{L}_\nu(\nu, u)\,\boldsymbol{\eta}\,\nu' + \mathbf{L}_u(\nu, u)\,\boldsymbol{\eta} \\ 2\boldsymbol{\eta}^{\mathsf{H}}\,\boldsymbol{\eta}' \end{bmatrix}. \tag{28}$$

Substituting the above expressions into

$$\mathbf{f}'(\boldsymbol{\eta}, \nu, u) = -\chi\mathbf{f}(\boldsymbol{\eta}, \nu, u), \tag{29}$$

we obtain the system of ODEs[6]

$$\begin{bmatrix} \mathbf{L}(\nu, u) & \mathbf{L}_\nu(\nu, u)\,\boldsymbol{\eta} \\ 2\boldsymbol{\eta}^{\mathsf{H}} & 0 \end{bmatrix} \begin{bmatrix} \boldsymbol{\eta}' \\ \nu' \end{bmatrix} = -\chi \begin{bmatrix} \mathbf{L}(\nu, u)\,\boldsymbol{\eta} \\ \boldsymbol{\eta}^{\mathsf{H}}\boldsymbol{\eta} - 1 \end{bmatrix} - \begin{bmatrix} \mathbf{L}_u(\nu, u)\,\boldsymbol{\eta} \\ 0 \end{bmatrix}. \tag{30}$$

The partial derivatives of the terms on the right-hand side of Eq. (30) lead to the Jacobian that is required, or at least beneficial, for many algorithms solving initial value problems:

$$\mathbf{J}(\boldsymbol{\eta}, \nu, u) = -\begin{bmatrix} \chi\mathbf{L}(\nu, u) + \mathbf{L}_u(\nu, u) & \chi\mathbf{L}_\nu(\nu, u)\,\boldsymbol{\eta} + \mathbf{L}_{u\nu}(\nu, u)\,\boldsymbol{\eta} \\ 2\chi\boldsymbol{\eta}^{\mathsf{H}} & 0 \end{bmatrix}. \tag{31}$$

We list the derivatives used above for easier reference, though they are straightforward to obtain:

$$\mathbf{L}(\nu, u) = \nu^2\mathbf{M} + \nu\mathbf{C}(u) + \mathbf{K}(u), \tag{32}$$

$$\mathbf{L}_\nu(\nu, u) = 2\nu\mathbf{M} + \mathbf{C}(u), \tag{33}$$

$$\mathbf{L}_u(\nu, u) = 2\nu\sqrt{\beta}\mathbf{B} + 2\,u\mathbf{G}, \tag{34}$$

$$\mathbf{L}_{u\nu}(\nu, u) = 2\sqrt{\beta}\mathbf{B}. \tag{35}$$

With these expressions, Eq. (30) can be solved, starting from some initial solution of the eigenvalue problem at an arbitrary value of u.

[5] The term $\boldsymbol{\eta}^{\mathsf{H}}\boldsymbol{\eta}$ is not complex differentiable; however, $2\boldsymbol{\eta}^{\mathsf{H}}$ serves as a suitable approximation of a slope to be used in a minimization problem as discussed in [20,30].

[6] It is sometimes beneficial to use different decay parameters for the eigenvalue problem and the normalization of $\boldsymbol{\eta}$; see [30] for details. For the comparably basic problem solved here, we use only one parameter for the sake of conciseness.

We employ a Runge-Kutta method with a variable step size designed for stiff differential equations, specifically the one implemented in the Matlab function *ode15s*. A minor numerical issue can occur around points where an eigencurve is not continuously differentiable, which typically happens when a complex-valued eigenvalue becomes purely real. In the current application, we circumvent this problem by simply adding a small imaginary perturbation to the matrix $\mathbf{A}$; specifically, we use $\mathbf{A}(1 + \mathrm{i}10^{-4})$, hence avoiding sudden transitions to real eigenvalues without significantly deteriorating the accuracy of the solution.

6. Numerical examples

6.1. Eigencurves and critical points

We present in this section the results of four numerical examples with different values of β and γ. Varying β allows us to study the influence of the masses of the fluid and pipe material, whereas γ is related to the ratio of gravitational load to bending stiffness. The examples are the same as those used by Wagner et al. in [11] in order to allow easier comparison and verification. For a more detailed discussion of the physical behavior and the influence of varying the different parameters, the interested reader is referred to [1] and the references therein. The main difference to [11] is that we use our approach to compute the critical points directly, rather than following the eigencurve in order to find solutions with a vanishing real part. In addition, we employ the method based on exponential residual relaxation to compute selected eigencurves. The parameters of each example are summarized in Table 1. There, we also present the numerical values of critical velocities u_c and corresponding eigenvalues ν_c, computed using the proposed approach from Section 4, as well as the critical values published in [11] for comparison. The results using the two methods are in excellent agreement. Our results were computed using only one element with polynomial basis functions of order 15, resulting in 14 degrees of freedom after incorporating the Dirichlet boundary conditions. This discretization is sufficient to converge all digits of the solution presented in the table. The operator determinants are of size 392×392, and their eigenvalues can be computed without much effort. The computational time was about 0.3 s (in a Matlab environment on a laptop computer using an Intel Core Ultra 9 processor) for the direct computation of the critical points in all examples.

Eigencurves of the same four examples are shown in Figs. 3 and 4. We present both the real and imaginary parts of the eigenvalues as functions of the flow velocity. In addition, graphs of $\Im(\nu)$ versus $\Re(\nu)$ are included to allow a direct comparison with the data provided in [11]. Note that we only plot the eigenvalues with an imaginary part $\Im(\nu) < 70$. Additional spurious or non-converged modes exist that would otherwise be visible in the plots of the real part. Our results for the eigencurves are obtained by solving the quadratic eigenvalue problem for ν once at the maximum u-value of interest and following the curves backward towards $u = 0$ using the exponential residual relaxation. We chose the relative tolerance of the *ode15s* solver to be 10^{-4} and the decay parameter $\chi = 10$ in all examples. However, the algorithm works robustly for a wide range of χ-values; for details, we refer to [30]. With the selected

Table 1
Parameters γ, β of the numerical studies and results for the critical eigenvalues ν_c and critical velocities u_c. The critical velocities are compared with the values provided in [11].

γ	β	ν_c	u_c	u_c [11]
0	0.615	$\pm 26.2921i$	10.1062	10.110
0	0.380	$\pm 25.7750i$	8.6837	8.686
10	0.400	$\pm 27.9144i$	9.1892	9.190
–10	0.200	$\pm 12.3908i$	4.8659	4.868
		$7.1 \cdot 10^{-9}$	1.7972	1.796

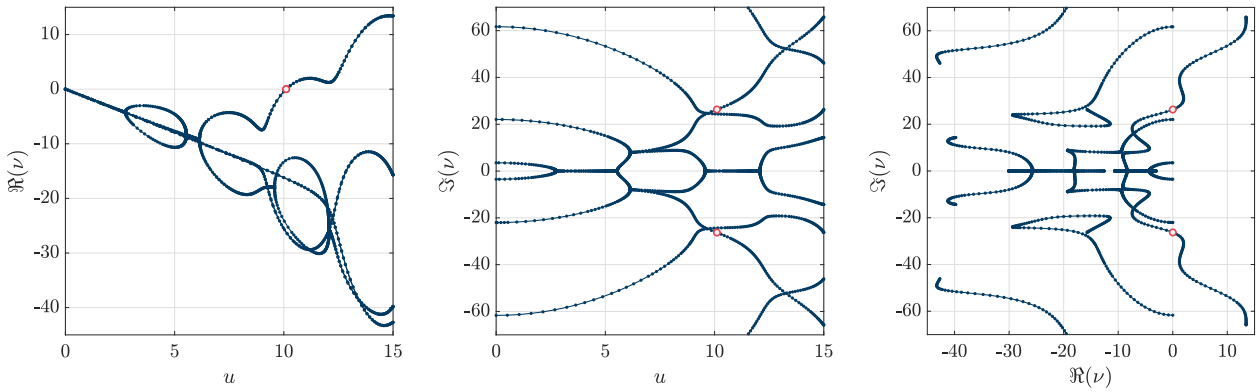

(a) $\gamma = 0$, $\beta = 0.615$

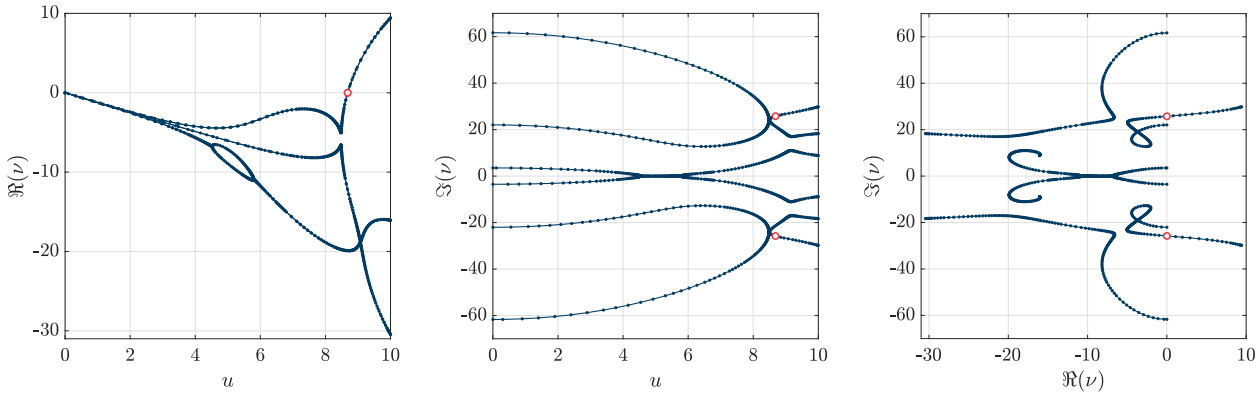

(b) $\gamma = 0$, $\beta = 0.38$

Fig. 3. Eigencurves (–●–) and critical points (∘) corresponding to the first two examples in Table 1.

settings, the computing time for an individual mode was about 0.15 s with an average of about 200 steps.

Lastly, Fig. 5 shows a detail of the eigencurves in the second example to demonstrate the effect of the perturbation as mentioned at the end of Section 5. To this end, we zoom in on a small range of u-values between 5.77 and 5.795 and compare the solution obtained by exponential residual relaxation with the one obtained by directly solving the quadratic eigenvalue problem (9) at 2000 values in the given range. Note that the shown detail includes a point where two eigencurves cross, and neither is continuously differentiable. Employing the exponential residual relaxation with the mentioned perturbation $\mathbf{A}(1 + \mathrm{i}10^{-4})$ yields a smooth approximation of the eigencurves with minor deviations from the exact solution.

6.2. Convergence study

To ensure the correctness of our results and, at the same time, assess the effect of employing the two different types of basis functions as described in Section 3.2, we conducted a convergence study by computing eigenvalues at $u = 10$ for each example using different discretizations and evaluating the numerical error of the results. Specifically, we included the first eight eigenvalues and compared the numerical results to a reference solution $\bar{\nu}_i$, defining the error

$$e = \sqrt{\frac{\sum_{i=1}^{8} (\nu_i - \bar{\nu}_i)^2}{\sum_{i=1}^{8} \nu_i^2}}. \tag{36}$$

The reference solution is obtained in two different ways, depending on the example. If $\gamma = 0$ (as in the first two examples), we can employ an analytical formulation as described in A. More precisely, we derive a transcendental equation whose roots are the sought eigenvalues. While it is challenging to find solutions to this equation without prior knowledge of their approximate values, we can use it to verify our numerical solutions. To this end, we treat our computed eigenvalues as initial guesses to find the closest exact solution of the transcendental equation using a numerical minimization algorithm. For the last two examples, no analytical solution is available, and we resort instead to a sufficiently converged finite-element solution. Fig. 6 shows the results for the second and fourth examples (the remaining two are similar and omitted for the sake of brevity). In the figures, 'beam modes' refers to the discretization using the eigenmodes of the Euler-Bernoulli beam as basis functions. The other results use the polynomial basis functions (Section 3.2), with $p = 3, 5, 7$ indicating the polynomial degree. Hence, in these cases, convergence is achieved by successively increasing the number of elements ('h-refinement'). In addition, we show the results of using only one element and increasing its polynomial degree ('p-refinement'). The polynomial basis functions behave as expected; calculating the slope based on the last two points on each graph, we obtain convergence rates of $2p - 2$ as predicted by finite element theory for eigenvalues using C^1-continuous elements. We also observe the typical exponential convergence using p-refinement. It is interesting to see that the beam modes perform quite well and, for smaller matrix sizes/larger errors, even outperform high-order polynomials. Nevertheless, their asymptotic convergence rate is only similar to that of third-order polynomials. Another, perhaps unexpected, result is that we obtain very similar errors across the different examples. In particular, one may have expected the beam modes to perform poorly for $\gamma > 0$ as this gives rise to additional terms in the ODE, including one proportional to ξ, which changes the mode shapes quite significantly.

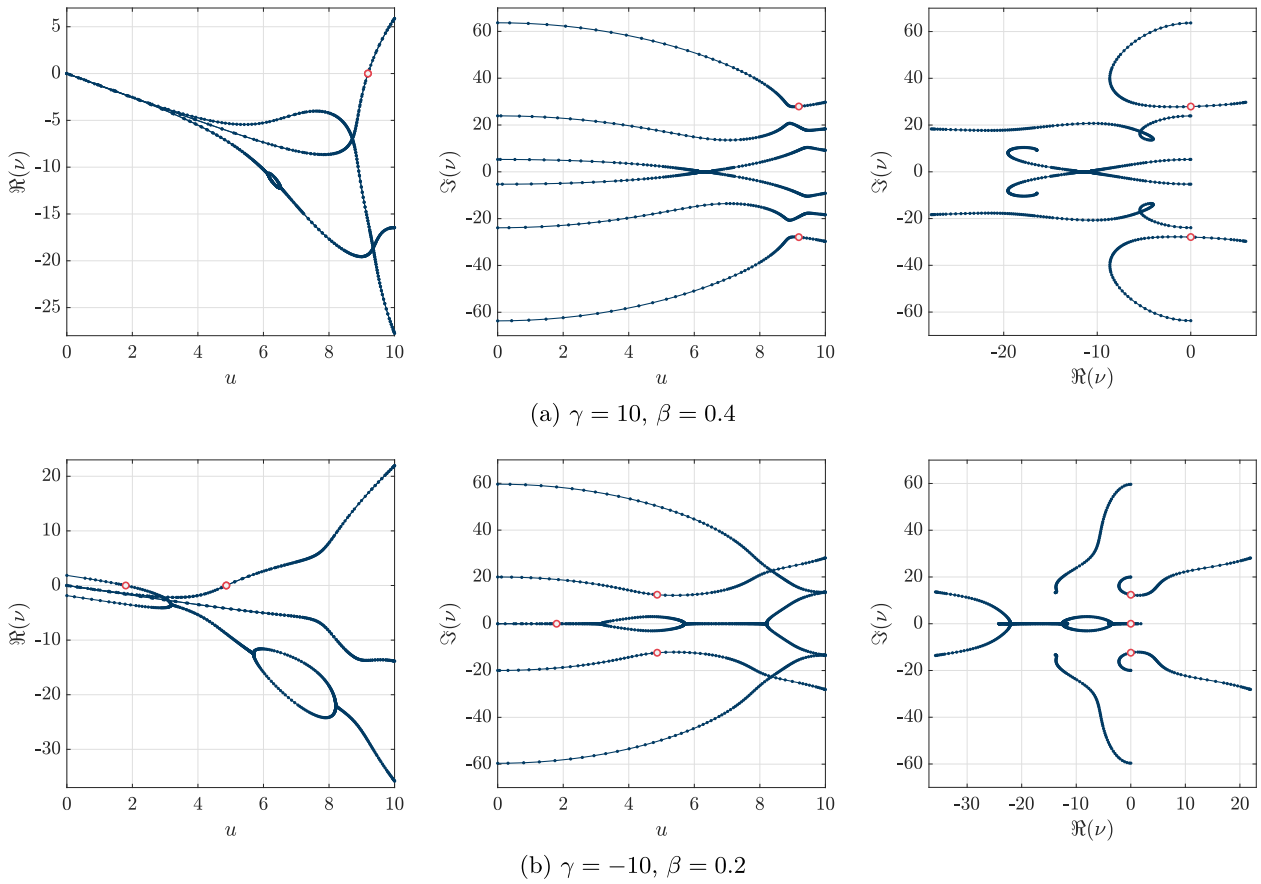

Fig. 4. Eigencurves (–●–) and critical points (∘) corresponding to the last two examples in Table 1.

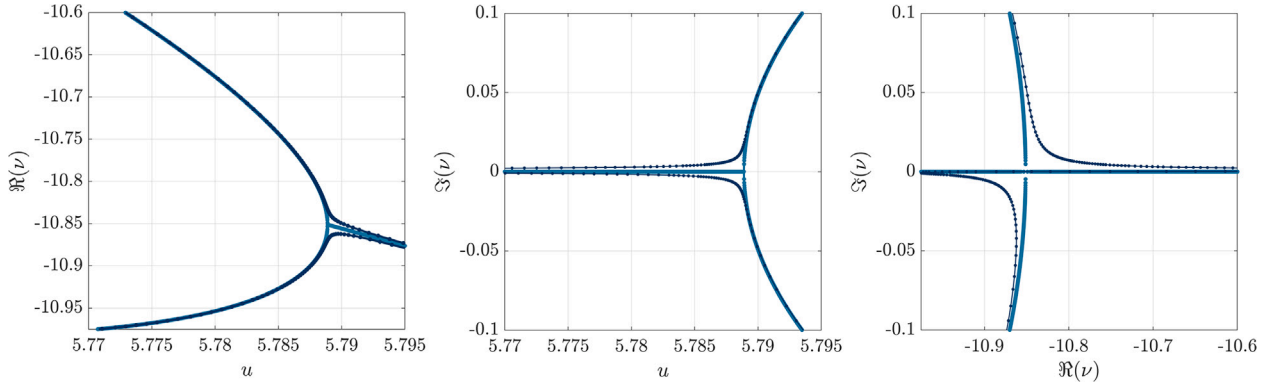

Fig. 5. Exemplary eigencurves involving discontinuous derivatives for the second example computed using exponential residual relaxation (–●–) and direct solution of the QEP (●).

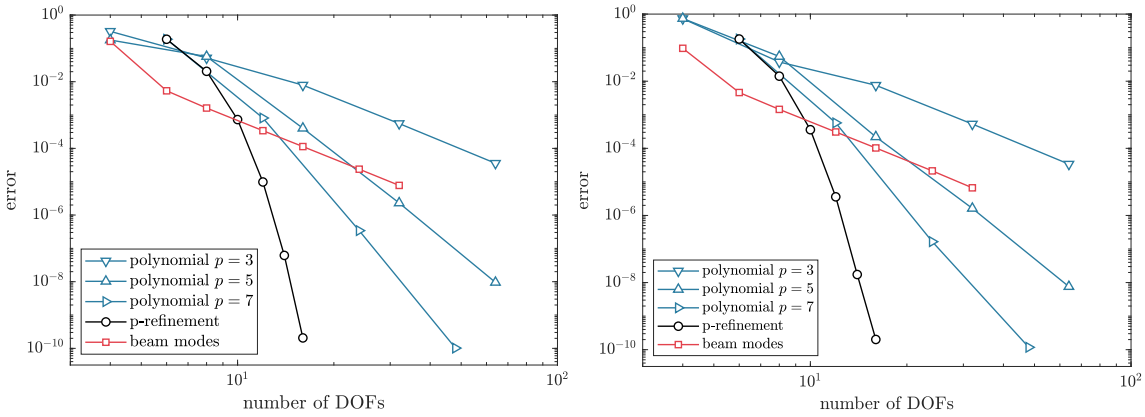

Fig. 6. Error convergence of the first eight eigenvalues for examples 2 and 4.

7. Conclusions

We have shown that the critical points in the investigated case of fluid-conveying pipes can be computed efficiently and accurately in a direct manner as solutions of a three-parameter eigenvalue problem. Furthermore, the method of *exponential residual relaxation* was capable of robustly following individual eigencurves. Regarding the discretization of the weak form, we recommend employing the recently developed high-order spectral elements of the Hermite type to minimize the required number of degrees of freedom. While we addressed a specific physical setup in this work, the presented techniques are quite general and will hopefully be applied to similar problems involving challenging parameter-dependent eigenvalue problems and other systems involving instabilities or different exceptional points.

CRediT authorship contribution statement

Hauke Gravenkamp: Writing – original draft, Visualization, Software, Methodology, Investigation, Conceptualization. **Bor Plestenjak:** Writing – review & editing, Methodology, Formal analysis.

Declaration of competing interest

The authors declare that they have no known competing financial interests or personal relationships that could have appeared to influence the work reported in this paper.

Acknowledgments

The second author has been partially supported by the Slovenian Research and Innovation Agency (grant P1-0294).

Appendix A. Analytical formulation for $\gamma = 0$

If $\gamma = 0$, the differential Eq. (1) simplifies significantly as the term in $\xi\eta''$ vanishes. In this case, we can obtain an analytical formulation for the eigenvalues ν at a given velocity u. That is to say, we can derive an exact transcendental equation for ν based on the strong form of the governing equation without requiring spatial discretization. The transcendental equation still requires a numerical algorithm to solve, just as in the case of the Euler-Bernoulli beam. Substituting $\gamma = 0$, the governing equation reads

$$\eta'''' + u^2\eta'' + 2\sqrt{\beta}u\nu\eta' + \nu^2\eta = 0.$$

Assuming a solution of the form $\mathrm{e}^{\lambda\xi}$ leads to the characteristic polynomial

$$\lambda^4 + u^2\lambda^2 + 2\sqrt{\beta}u\nu\lambda + \nu^2 = 0 \tag{A.1}$$

that defines the relationship between λ and ν. Since the polynomial has four roots, the general solution for given u and ν is $\eta(\xi) = \sum_{i=1}^{4} c_i \mathrm{e}^{\lambda_i \xi}$. Enforcing the boundary conditions, in our case

$$\eta(0) = \sum c_i = 0, \qquad \eta'(0) = \sum \lambda_i c_i = 0,$$
$$\eta''(1) = \sum \lambda_i^2 c_i \mathrm{e}^{\lambda_i} = 0, \qquad \eta'''(1) = \sum \lambda_i^3 c_i \mathrm{e}^{\lambda_i} = 0 \tag{A.2}$$

defines the constants c_i via

$$\mathbf{T}(\lambda(\nu))\mathbf{c} = \begin{bmatrix} 1 & 1 & 1 & 1 \\ \lambda_1 & \lambda_2 & \lambda_3 & \lambda_4 \\ \lambda_1^2\mathrm{e}^{\lambda_1} & \lambda_2^2\mathrm{e}^{\lambda_2} & \lambda_3^2\mathrm{e}^{\lambda_3} & \lambda_4^2\mathrm{e}^{\lambda_4} \\ \lambda_1^3\mathrm{e}^{\lambda_1} & \lambda_2^3\mathrm{e}^{\lambda_2} & \lambda_3^3\mathrm{e}^{\lambda_3} & \lambda_4^3\mathrm{e}^{\lambda_4} \end{bmatrix} \begin{bmatrix} c_1 \\ c_2 \\ c_3 \\ c_4 \end{bmatrix} = \begin{bmatrix} 0 \\ 0 \\ 0 \\ 0 \end{bmatrix}, \tag{A.3}$$

where we denote the vector of all integration constants by $\mathbf{c}$, and λ is the collection of all four solutions of λ. The above equation has nontrivial solutions if

$$\det(\mathbf{T}(\lambda(\nu))) = 0. \tag{A.4}$$

Hence, (A.4) is the sought transcendental equation that can be solved numerically for ν to obtain eigenvalues at a given value of u. In general, the solution of (A.4) requires, in each iteration, a solution of (A.1), i.e., the computation of the four roots of the characteristic equation. This is usually best done numerically. However, we may note that, if the problem is further simplified by setting $\beta = \gamma = 0$, these four solutions are obtained in closed form as

$$\lambda_{1,2,3,4} = \pm\sqrt{-\frac{u^2}{2} \pm \sqrt{\frac{u^4}{4} - \nu^2}}. \tag{A.5}$$

Finally, let us remark that for $\beta = \gamma = u = 0$, we recover the standard Euler-Bernoulli beam modes with

$$\lambda^4 = -\nu^2 = \omega^2 \tag{A.6}$$

with real-valued frequencies ω, in which case the solution can be rewritten in the form already shown in Eq. (13).

Finding *all* solutions of Eq. (A.4) within given intervals for u and ν can be a rather challenging endeavour in the general case.[7] Hence, for practical purposes, the discretization of the eigenvalue problem as done in this paper is much preferred. Nevertheless, the analytical expression is particularly useful for verifying the numerical solutions. To this end, we use our numerical solutions as starting values and minimize Eq. (A.4) to find the closest analytical solution with sufficient precision. In this way, we can reliably determine the error in our numerical computations.

[7] One may note that a similar problem occurs in computing the elastic guided wave modes in plates and cylinders, which has given rise to a substantial body of literature on the robust solution of similar transcendental equations.

Data availability

Data will be made available on request.

References

[1] Païdoussis MP, Issid NT. Dynamic stability of pipes conveying fluid. J Sound Vib 1974;33(3):267–94. https://doi.org/10.1016/S0022-460X(74)80002-7

[2] Holmes PJ. Bifurcations to divergence and flutter in flow-induced oscillations: a finite dimensional analysis. J Sound Vib 1977;53(4):471–503. https://doi.org/10.1016/0022-460X(77)90521-1

[3] Wang Y-X, Tang Y, Yang T-Z. Nonlinear mechanic analysis of a composite pipe conveying solid-liquid two-phase flow. Appl Ocean Res 2024;144:103905. https://doi.org/10.1016/j.apor.2024.103905

[4] Szmidt T, Konowrocki R, Pisarski D. Stabilization of a cantilever pipe conveying fluid using electromagnetic actuators of the transformer type. Meccanica 2021;56(12):2879–92. https://doi.org/10.1007/s11012-021-01419-y

[5] Tang Y, Zhang H-J, Chen L-Q, Ding Q, Gao Q, Yang T. Recent progress on dynamics and control of pipes conveying fluid. Nonlinear Dyn 2025;113(7):6253–315. https://doi.org/10.1007/s11071-024-10486-1

[6] Wagner N, Gaul L. Stability analysis of gyroscopic systems via quadratic matrix equations, In: 7th IFToMM-Conference on Rotor Dynamics; Vienna, Austria; 2006. p. 87.00.

[7] Bajaj AK, Sethna PR, Lundgren TS. Hopf bifurcation phenomena in tubes carrying a fluid. SIAM J Appl Math 1980;39(2):213–30. https://doi.org/10.1137/0139019

[8] Sarkar A, Paidoussis MP. A compact limit-cycle oscillation model of a cantilever conveying fluid. J Fluids Struct 2003;17(4):525–39. https://doi.org/10.1016/S0889-9746(02)00150-0

[9] Yamashita K, Nishiyama N, Katsura K, Yabuno H. Hopf-Hopf interactions in a spring-supported pipe conveying fluid. Mech Syst Signal Process 2021;152:107390. https://doi.org/10.1016/j.ymssp.2020.107390

[10] Feng C, Li Y-D, Ou G-Y. Hopf bifurcation of a standing cantilever pipe conveying fluid with time delay. Math Probl Eng 2022;2022:1–15. https://doi.org/10.1155/2022/3588068

[11] Wagner N, Gaul L. Parameter-dependent matrix eigenvalue problems and their applications in structural dynamics, In: EURODYN International Conference on Structural Dynamics; 2005. p. 2183–8.

[12] Guckenheimer J, Myers M, Sturmfels B. Computing Hopf bifurcations I. SIAM J Numer Anal 1997;34(1):1–21. https://doi.org/10.1137/S0036142993253461

[13] Bora N, Chutia B, Bhattacharyya S. On multiparameter spectral theory of 3-parameter aeroelastic flutter problems. Int J Appl Math 2023;53(4) IJAM_53_4_19.

[14] Pons A, Gutschmidt S. Multiparameter solution methods for semistructured aeroelastic flutter problems. AIAA J 2017;55(10):3530–8. https://doi.org/10.2514/1.J055447

[15] Pons A, Gutschmidt S. Multiparameter spectral analysis for aeroelastic instability problems. J Appl Mech 2018;85(61011):1–10. https://doi.org/10.1115/1.4039671

[16] Pons A, Gutschmidt S. Nonlinear multiparameter eigenvalue problems in aeroelasticity. Int J Struct Stab Dyn 2019;19(5):1941008. https://doi.org/10.1142/S0219455419410086

[17] Hochstenbach ME, Košir T, Plestenjak B. A Jacobi-Davidson type method for the two-parameter eigenvalue problem. SIAM J Matrix Anal Appl 2004;26(2):477–97. https://doi.org/10.1137/S0895479802418318

[18] Muhič A, Plestenjak B. On the quadratic two-parameter eigenvalue problem and its linearization. Linear Algebra Appl 2010;432(10):2529–42. https://doi.org/10.1016/j.laa.2009.12.022

[19] Plestenjak B. MultiParEig. 2023. www.mathworks.com/matlabcentral/fileexchange/47844-multipareig.

[20] Kiefer DA, Plestenjak B, Gravenkamp H, Prada C. Computing zero-group-velocity points in anisotropic elastic waveguides: globally and locally convergent methods. J Acoust Soc Am 2023;153(2):1386–98. https://doi.org/10.1121/10.0017252

[21] Plestenjak B, Kiefer DA, Gravenkamp H. A Sylvester equation approach for the computation of zero-group-velocity points in waveguides. Comput Mech 2025. https://doi.org/10.1007/s00466-025-02656-8

[22] Gravenkamp H, Plestenjak B, Kiefer DA, Jarlebring E. Computation of leaky waves in layered structures coupled to unbounded media by exploiting multiparameter eigenvalue problems. J Sound Vib 2025;596:118716. https://doi.org/10.1016/j.jsv.2024.118716

[23] Zhang Y, Wang J. Recurrent neural networks for nonlinear output regulation. Automatica 2001;37(8):1161–73. https://doi.org/10.1016/S0005-1098(01)00092-9

[24] Zhang Y, Jiang D, Wang J. A recurrent neural network for solving Sylvester equation with time-varying coefficients. IEEE Trans Neural Netw 2002;13(5). https://doi.org/10.1109/TNN.2002.1031938

[25] Zhang Y, Ge SS. Design and analysis of a general recurrent neural network model for time-varying matrix inversion. IEEE Trans Neural Netw 2005;16(6):1477–90. https://doi.org/10.1109/TNN.2005.857946

[26] Uhlig F, Zhang Y. Time-varying matrix eigenanalyses via Zhang neural networks and look-ahead finite difference equations. Linear Algebra Appl 2019;580:417–35. https://doi.org/10.1016/j.laa.2019.06.028

[27] Uhlig F. Zhang neural networks for fast and accurate computations of the field of values. Linear and Multilinear Algebra 2020;68(9):1894–910. https://doi.org/10.1080/03081087.2019.1648375.

[28] Uhlig F. Zhang neural networks: an introduction to predictive computations for discretized time-varying matrix problems. Numer Math 2024;156:691–739. https://doi.org/10.1007/s00211-023-01393-5

[29] Gravenkamp H, Plestenjak B, Kiefer DA. Notes on osculations and mode tracing in semi-analytical waveguide modeling. Ultrasonics 2023;135:107112. https://doi.org/10.1016/j.ultras.2023.107112

[30] Gravenkamp H, Plestenjak B, Kiefer DA. Computing leaky waves in semi-analytical waveguide models by exponential residual relaxation. arxiv E-Prints 2025. https://doi.org/10.48550/arXiv.2505.04735

[31] Gravenkamp H, Song C, Prager J. A numerical approach for the computation of dispersion relations for plate structures using the scaled boundary finite element method. J Sound Vib 2012;331(11):2543–57. https://doi.org/10.1016/j.jsv.2012.01.029

[32] Gravenkamp H, Man H, Song C, Prager J. The computation of dispersion relations for three-dimensional elastic waveguides using the scaled boundary finite element method. J Sound Vib 2013;332:3756–71. https://doi.org/10.1016/j.jsv.2013.02.007

[33] Kapuria S, Jain M. A C1-continuous time domain spectral finite element for wave propagation analysis of Euler–Bernoulli beams. Int J Numer Methods Eng 2021;122(11):2631–52. https://doi.org/10.1002/nme.6612

[34] Eisenträger S, Kapuria S, Jain M, Zhang J. On the numerical properties of high-order spectral (Euler-Bernoulli) beam elements. ZAMM J Appl Math Mech 2023;103(9):e202200422. https://doi.org/10.1002/zamm.202200422

[35] Nennig B, Perrey-Debain E. A high order continuation method to locate exceptional points and to compute Puiseux series with applications to acoustic waveguides. Journal of Computational Physics 2020;412:109425. https://doi.org/10.1016/j.jcp.2020.109425.

[36] Patera AT. A spectral element method for fluid dynamics: laminar flow in a channel expansion. J Comput Phys 1984;54(3):468–88. https://doi.org/10.1016/0021-9991(84)90128-1

[37] Cohen G, Joly P, Tordjman N. Higher-order finite elements with mass-lumping for the 1D wave equation. Finite Elem Anal Des 1994;16:329–36. https://doi.org/10.1016/0168-874X(94)90075-2

[38] Tschöke K, Gravenkamp H. On the numerical convergence and performance of different spatial discretization techniques for transient elastodynamic wave propagation problems. Wave Motion 2018;82:62–85. https://doi.org/10.1016/j.wavemoti.2018.07.002

[39] Hochstenbach ME, Muhič A, Plestenjak B. On linearizations of the quadratic two-parameter eigenvalue problem. Linear Algebra Appl 2012;436:2725–43. https://doi.org/10.1016/j.laa.2011.07.026

[40] Atkinson FV. Multiparameter eigenvalue problems vol I: matrices and compact operators, vol. 82 of mathematics in science and engineering. New York-London: Academic Press; 1972.

[41] Hartshorne R. Algebraic Geometry, Graduate Texts in Mathematics. 1st ed. Springer New York; 1977.

[42] Meerbergen K, Spence A. Inverse iteration for purely imaginary eigenvalues with application to the detection of Hopf bifurcations in large-scale problems. SIAM J Matrix Anal Appl 2010;31(4):1982–99. https://doi.org/10.1137/080742890